

Preparation of semi-hydrogenation catalysts by embedding Pd in layered double hydroxides nanocages via sacrificial template of ZIF-67

Peng Zhang^a, Ziyang Wang^a, Yan Zhang^a, Jian Wang^a, Wenqing Li^b, Lina Li^a, Peiping Zhang^a, Cundi Wei^a, Shiding Miao^{a,*}

^a Key Laboratory of Automobile Materials of Ministry of Education, Solid Waste Recycling Engineering Research Center of Jilin, School of Materials Science and Engineering, Jilin University, Changchun, 130022, Jilin Prov., China

^b Key Laboratory of Mineral Resources Evaluation in Northeast Asia, Ministry of Land and Resources, Changchun 130061, Jilin Prov., China

ARTICLE INFO

Keywords:

Palladium catalyst
Semi-hydrogenation
Layered double hydroxides
2-Methyl-3-butyn-2-ol
Selectivity

ABSTRACT

In this work a Pd/Fe-Co-Ni layered double hydroxide (LDH) composite was prepared and investigated in the semi-hydrogenation of 2-methyl-3-butyn-2-ol (MBY). Hollow nanocages of ternary Fe-Co-Ni LDH were constructed by stacking the LDH nanosheets edge-to-face which inherited the rhombic dodecahedral structure of ZIF-67 templates. Uniform palladium (Pd) nanocrystals with cubic shapes were imbedded in the LDH nanocages via a solvothermal method. The hydroxyl groups on LDH supports were critical to inhibit the association of excess hydrogen atoms on the catalyst, so less MBY molecules were converted to 2-methyl-2-butanol (MBA) during the hydrogenation catalysis. Under optimized reaction conditions the hydrogenation activity of Pd/Fe-Co-Ni LDH was significantly improved, and the conversion of MBY was higher than 99% with selectivity of 2-methyl-3-buten-2-ol (MBE) exceeding 99%. The catalyst was easily recovered and had little reduction in catalytic performance during the cycling reactions.

1. Introduction

Catalytic hydrogenation of acetylenic alcohols to alkenols is a key step for fine chemicals and intermediate products. One example is the hydrogenation of 2-methyl-3-butyn-2-ol (MBY) to 2-methyl-3-buten-2-ol (MBE), which is critical for synthesis of vitamins, fragrances and agrochemicals, and has been conducted over lead (Pb)-poisoned palladium (Pd) supported on calcium carbonate (CaCO₃) as current Lindlar catalysts [1,2]. Lindlar catalysts (Pd-Pb/CaCO₃) were widely used due to its high selectivity toward semi-hydrogenation [3]. However, drawbacks were found as toxicity of Pb, necessity of adding quinolone, and instability of CaCO₃ supports, which resulted in harmful and irreversible chemical transformations [4,5]. Various strategies have been proposed to replace the lead poisoned Lindlar catalysts and to regulate catalytic activity as well for special use in semi-hydrogenation [6,7]. Selecting metallic palladium as catalysts for semi-hydrogenation was preferred due to the stronger adsorption of alkynes compared to interaction of alkene on the surface of Pd particles, which was caused by the high electron density and restricted rotation of carbon-carbon triple bonds [8]. However, the Pd(0) nanocrystals (NCs) would aggregate due to the high surface energy caused by their nano-size nature. The heterogeneous catalyst which contains Pd NCs and porous supports would

be an ideal choice for preventing NCs agglomeration. Mesoporous supports with different levels of pores would save the dosage amount of novel metals by providing enough surface areas. Sometimes there were special interactions occurs between catalytic species and supports, which would benefit the catalytic performance by the so-called synergistic effects [9]. For instance, the palladium supported on N-doped carbons [10], metal-organic frameworks [11], inorganic materials (ZnO) [12], organic materials (polymers, resins, organic frameworks) [13], and metallic/non-metallic (Pd-Zn, Pd-Si, etc.) alloys have been found as catalysts in hydrogenation of acetylenic alcohols [14–19]. Although homogeneous Pd catalysts were found to show excellent selectivity in the semi-hydrogenation of MBY [20], there still remained some shortages. The high costs and difficulty in separation were always encountered, and in most cases the high catalytic activity of Pd resulted in over-hydrogenation. To solve the problem of over-hydrogenation, poisoning or isolation was used to reduce activity of Pd NCs. The facet sites of Pd NCs were assumed to be active sites for semi-hydrogenation, and sites from corners and edges were responsible for over-hydrogenation [21]. Hydrogenation of acetylenic alcohol was demonstrated not only to be a structure-sensitive reaction but also a size-independent on Pd particles (6–13 nm). The particle size did not affect selectivity to MBE, but did affect the formation of dimers and saturated by-products,

* Corresponding author.

E-mail addresses: miaosd@jlu.edu.cn, miaosd@iccas.ac.cn (S. Miao).

<https://doi.org/10.1016/j.apcata.2020.117540>

Received 12 December 2019; Received in revised form 15 March 2020; Accepted 21 March 2020

Available online 10 April 2020

0926-860X/ © 2020 Elsevier B.V. All rights reserved.

i.e., the larger particle size the lower ratio of dimers to MBA obtained [22]. It is desirable to prepare Pd catalysts with appropriate size and specific morphologies that have different types of active sites, e.g., planes, corners and edges to fulfill the semi-hydrogenation catalysis.

Usually a corner position in catalysts was designed to improve the catalytic activity, and the carrier was used to prevent over-hydrogenation. The Brønsted base, e.g., $-OH$ was found to boost adsorption and activation of acetylenic alcohols. Mechanisms were identified by the high basicity of ligands which increased electron density of catalyst center, functioned as electron donors, and thus the oxidative addition of H_2 was able to be accelerated. Examples were found as Brønsted bases being beneficial to increase 'electron' density of Pd surfaces, which decreased alkene adsorption, and resulted in a high yield of semi-hydrogenation [23]. However, the above conclusions were drawn from homogeneous catalysts in the semi-hydrogenation, and no trials were conducted by using of hard-templates with solid alkali as in forms of supports. Layered double hydroxides (LDH), known as brucite $Mg(OH)_2$ -like with intercalated anions (CO_3^{2-} , NO_3^- , OH^-) and water molecules confined in interlayer galleries, are a kind of basic materials with formula $[M_1^{2+}_x M_2^{3+}_y (OH)_2]^{z+} A_{z/n}^{n-} \cdot mH_2O$. The M^{2+} and M^{3+} represent divalent and trivalent metal cations (Fe^{3+} , Ni^{2+} , Co^{2+} , etc.), and are located in host layers with 'x' ranging 0.2~0.33 [24]. The LDH materials have been demonstrated as heterogeneous catalysts in photocatalysis, electrocatalysis, and thermocatalysis [25]. Due to the OH^- groups, LDHs were thought as suitable catalysts for hydrogenation of alkynes. The support induced self-poison/self-isolation, and will make Pb poisoning unnecessary in Lindlar catalysts. The combination use of Pd and LDHs have been observed to play an important role in tuning electronic structure of supported metal NCs [26]. The alkalinity was found to influence the mobility of Pd atoms, and thus prevent over-sintering during thermal treatments [27]. It was known that the activation of hydrogen on Pd catalysts involved a hybrid dissociation that produced a negatively charged $Pd-H\delta^-$. The positively charged $-H$ atoms were assumed to bond with $-OH$ groups. Although LDHs have 2D structures, the flexible composition and confinement effect make this type of materials serve as supports for noble metals, yet the limited specific area poses hindrance from their wide applications [28]. Therefore more efforts in preparing porosity with 3D hollow nanostructures have been developed to get higher specific areas [29]. The cavity constructed by packing LDH platelets would provide shorter diffusion paths for reactions, and thus affect the adsorption-desorption of substrate molecules. Recently Chen et al. [30], utilized zeolitic imidazolate framework-67 (ZIF-67) as templates to synthesize hollow LDH polyhedra via a sacrificial template method. Superior pseudocapacitance properties were obtained by benefiting from the larger specific area and hierarchical/submicroscopic 3D structures.

Owing to the special morphology of ZIF-67 as well as inspired by Chen's findings [30], we selected the micro-sized ZIF-67 particles as templates to synthesize Fe-Co-Ni LDH hollow nanocages. The composite Pd/Fe-Co-Ni LDH was prepared by embedding the pre-synthesized Pd NCs. The LDH nanocages inherited the ZIF-67 framework perfectly, and shells were composed of exfoliated LDH nanoflakes. The co-precipitation of Fe^{3+} , Co^{3+} and Ni^{2+} leads to formation of $[(Ni,Co)_{1-x}(Fe,Co)_x(OH)_2]^{z+}(NO_3^-)_z \cdot mH_2O$, in which the positive charge $z+$ was tunable by dosages of Fe^{3+} , Co^{3+} and Ni^{2+} . The composites were found to have sufficient active sites for catalysis. The performance was investigated by using Pd/Fe-Co-Ni LDH nanocages as catalysts in the semi-hydrogenation of MBY. Under pressure of $P_{H_2} = 0.5$ MPa at room temperature ($RT = \sim 60^\circ C$), the conversion of MBY reached almost $\sim 100\%$, and the selectivity of MBE was higher than 99% when reactions were conducted under solvent-free condition. This work validates that LDH can readily function as nanocages by deliberately controlling synthetic reaction kinetic balance between precipitation of shells and simultaneous etching of sacrificial templates [31]. The face-centered cubic of Pd NCs as catalytic species were successfully embedded in these LDH cages. The H_2 adsorption assisted by Brønsted-base could be activated on the Pd

NCs. The hydrogen atoms were indicated to diffuse into cages and form $-OH$ species followed by reacting with MBY. The target product MBE was obtained while restraining the yield of by-products.

2. Experimental

2.1. Chemicals and materials

Chemicals used in this research were provided by Aladdin-E.Com including $Co(NO_3)_2 \cdot 6H_2O$ (AR., $\geq 99.5\%$), 2-methylimidazole (short for 'mim', AR., $\geq 99.0\%$), $Fe(NO_3)_3 \cdot 9H_2O$ (AR), $Ni(NO_3)_2 \cdot 6H_2O$ (AR., $\geq 98\%$), sodium tetrachloropalladate (Na_2PdCl_4 AR., $\geq 98\%$), KCl (GR., 99.8%), KBr (AR., 99.0%), ascorbic acid (short for 'AA', AR. $> 99.0\%$), polyvinylpyrrolidone (58,000, K29-32, short for 'PVP'). 2-Methyl-3-butyn-2-ol (short for 'MBY', purum, $\geq 99\%$), 2-methyl-3-buten-2-ol (short for 'MBE', purum, $\geq 97\%$), and 2-methyl-2-butanol (short for 'MBA', purum, $\geq 98\%$). All chemicals were used without further purification.

2.2. Preparation of the Pd/Fe-Co-Ni LDH catalyst

2.2.1. Synthesis of ZIF-67

The rhombic dodecahedron ZIF-67 were synthesized via a modified method [32]. Typically, $Co(NO_3)_2 \cdot 6H_2O$ (1.0 mmol) and 2-methylimidazole (4.0 mmol) were dissolved in 25 mL methanol, respectively. The two solutions were homogenized via ultrasonication (~ 10 min, RT). The mixture was kept still for about 24 h to precipitate ZIF-67. The ZIF-67 particles were washed several times with methanol, and dried under vacuum ($60^\circ C$) prior for further use.

2.2.2. Synthesis of Pd NCs

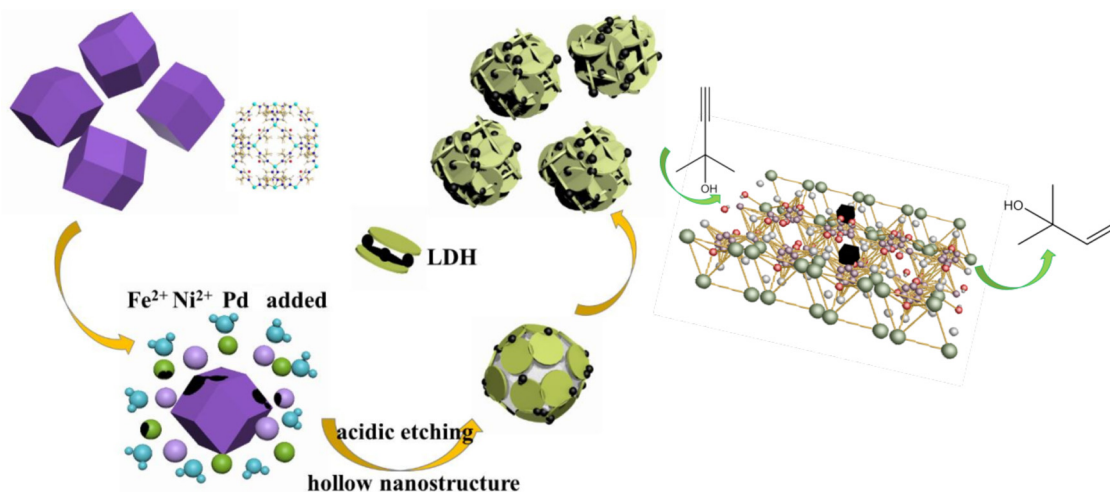
To ensure selectivity of the catalyst, the size of Pd NCs was synthesized at the size of ~ 10 nm as possible. The histogram of size distribution of Pd NCs was shown in Fig. S1. The Pd NCs were synthesized by mixing PVP (58,000 Mw, 105 mg), AA (60 mg), KBr (5 mg) and KCl (185 mg) dissolved in deionized water (8 mL) under magnetic stirring (~ 10 min, at RT). Another portion of Na_2PdCl_4 (57 mg) was dissolved in deionized water (3.3 mL). The two kinds of solution were mixed, and were kept under magnetic stirring for 3 h at $80^\circ C$. After reaction certain amount of acetone (~ 15 mL) was added to precipitate Pd NCs via centrifugation (11,000 rpm, ~ 20 min).

2.2.3. Syntheses of the catalyst Pd/Fe-Co-Ni LDH

To load Pd NCs within LDH, the as-prepared template (ZIF-67) was transferred into a round bottomed flask consisting with 0.01 g $Fe(NO_3)_3 \cdot 9H_2O$, 0.08 g $Ni(NO_3)_2 \cdot 6H_2O$ and 25.0 mL ethanol. The Pd NCs dispersed in methanol (4.0 wt.%) were added to the above ethanol solution. The mixture was treated via ultrasonication for 10 min, and was then refluxed at $80^\circ C$ for ca. 1 h. After the solvothermal treatment composites were collected by centrifugation, washed with anhydrous ethanol, and dried at $80^\circ C$ overnight. The schematic diagram of Pd/Fe-Co-Ni LDH nanocages were illustrated as Scheme 1. For comparison, the catalytic hydrogenations were also presented that were catalyzed by the same size of Pd NCs loaded on different supports, including ZIF-67, Co LDH, Co-Ni LDH, Fe-Co-Ni LDH been treated at $500^\circ C$, with co-precipitation of Fe-Co-Ni LDH, and several other inorganic oxide supported catalysts of commercial activated carbon (AC), $\gamma-Al_2O_3$ and SiO_2 . Results of the hydrogenation were listed in Table 2.

2.3. Characterizations

X-ray diffraction (XRD) patterns were collected on a Regaku D/max-5000 powder diffractometer equipped with $Cu K\alpha$ ($\lambda = 0.15418$ nm) radiation operating at 40 kV and 20 mA. Data were recorded within 2θ of $3-80^\circ$ at a speed of $0.05^\circ/20$ s per step. The morphology was examined by scanning electron microscope (SEM, Hitachi SU8020) and



Scheme 1. Schematic illustration of the fabrication of Pd/Fe-Co-Ni LDH nanocages and using as catalysts in hydrogenation of 2-methyl-3-butyn-2-ol (MBY).

transmission electron microscope (TEM, JEOL JEM-2100 F) with an accelerating voltage of 200 kV. The thermal behavior was investigated by using thermo gravimetric analysis (TG, Netzsch STA 449 F3 Jupiter) performed in N_2 atmosphere during heating steps. Samples of ~ 10 mg were loaded into the thermal analyzer, and were heated from RT to 1000 °C at 5 °C/min. To evaluate the specific surface area (SSA) and pore-size distribution, samples were degassed at 60 °C for 12 h prior to the N_2 adsorption-desorption, and this measurement was performed on a Micromeritics Tristar II 3020 M. The X-ray photoelectron spectrum (XPS) was recorded on a PHI-5300 ESCA spectrometer (Perkin Elmer) with its energy analyzer working in the pass energy mode at 30.0 eV, and the Al $K\alpha$ line was used as the excitation source. The binding energy of C1 s was shifted to 284.8 eV as the reference. The XPS profiles were deconvoluted by using an X-peak program with a Gaussian-Lorentzian mix function and Shirley background subtraction. Fourier transform infrared spectroscopy (FT-IR) was collected on a Bruker IFS 66 v/s spectrometer (linked with an in-situ test apparatus) which was registered between 4000 and 400 cm^{-1} with 128 scans per spectrum. Temperature-programmed desorption of hydrogen (H_2 -TPD) was measured by using a Micromeritics ChemiSorb 2920 equipped with an on-line mass spectrometry, and a thermal conductivity detector (TCD). The Pd content was determined by inductively coupled plasma atomic emission spectroscopy (ICP-AES, Thermo Scientific).

2.4. Catalytic performance measurements

The catalytic performance on hydrogenation of MBY was evaluated in a 50 mL stainless vessel equipped with a magnetic stirrer heating jacket and a Parr high-pressure hydrogen supply system. In a typical process 10.0 mg of catalyst was mixed with 5.0 mL of MBY, and were introduced into the vessel. The reactor was flushed vacuum/ H_2 alternatively to remove air inside for four cycles, and heated up to the target temperature within 20 min. During the reaction the reactor was carried out at desired pressure of H_2 and under intensive stirring ~ 2000 rpm. The starting reaction time was recorded at the point when the above conditions were achieved. When the reaction was completed, the device was cooled in an ice bath and depressurized. Samples were periodically withdrawn from the reactor, and were analyzed by gas chromatography (GC, SP-6890) equipped with a FAAP column (30 m, 0.25 mm) and an FID detector. The injector and flame ionization detector temperatures were set at 200 °C and 250 °C, respectively. The oven temperature was maintained at 50 °C for 5 min, and increased to 200 °C at a ramp rate of 2 °C/min. Due to the fact that only MBY, MBE and MBA were included in our system, and the carbon balance was evaluated to be $100 \pm 2\%$ according to the weight assessment [33]. Quantities of reactant/

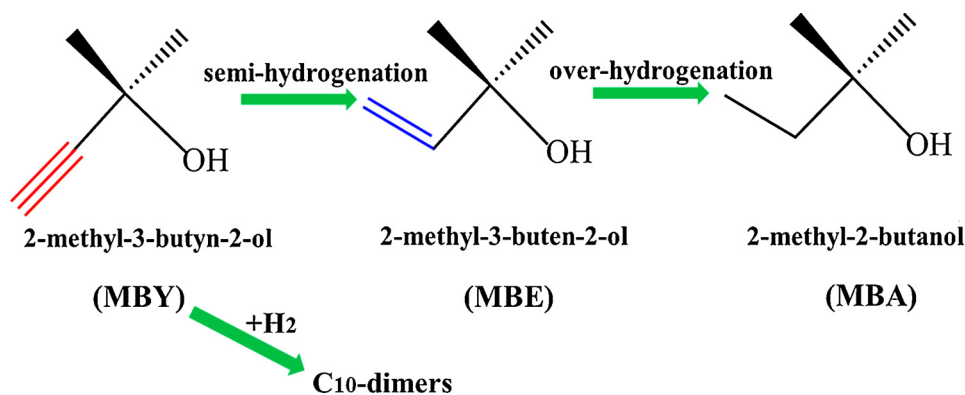
products were evaluated by the GC factor of a certain component which was obtained by known weight of standard substance to the internal standard (n-hexane) according to GC analysis. By adding a certain amount of n-hexane to a sample mixture with known weight, the GC factor for a certain substance was obtained by the peak ratio of integrated area of internal standard to those tested components based on the chromatographic profiles. By considering the GC factor, the percentage of each measured component can be achieved. The yield of each component Y_i (where 'i' represented MBY, MBE, MBA [34], and others, e.g., dimmers [35]) was calculated from peak areas of the GC signal factors. Selectivity to MBE, MBA, and other was defined as $S_i = Y_i \times X \times 100\%$, where X was a MBY conversion. As a measure of activity, the turnover frequency (TOF) of MBY was calculated as conversion of moles of MBY per molar Pd in one second. To test the stability of catalysts, the mixture was recovered (Fig. S2) and reused. The diagram for hydrogenation of MBY was denoted as Scheme 2.

3. Results and discussion

3.1. Material characterizations

Fig. 1 presented XRD patterns of the pre-synthesized Pd NCs, template of ZIF-67, cages of LDH (Fe-Co-Ni LDH), and the final Pd/Fe-Co-Ni LDH composite after embedding with Pd NCs. The Pd NCs had three XRD reflections observed at $2\theta = 40^\circ, 46^\circ$ and 68° which could be indexed to (111), (200), and (220) planes of a face-centered cubic (fcc) Pd (0) (PDF 46-1043) [36]. The XRD pattern of ZIF-67 matched well with the simulated zeolitic imidazolate framework-67 published elsewhere [37], demonstrating the synthesized templates as phase-pure ZIF-67. For the hydrothermal synthesized LDH, i.e., the sample of Fe-Co-Ni LDH was prepared by sacrificing ZIF-67 frameworks. Three conspicuous diffraction peaks at 2θ values of $11.7^\circ, 23.5^\circ$, and 34.6° were assigned to reflections of plan (003), (006) and (012) of the LDH phase [38]. The basal spacing of LDH could be calculated from plane (003) reflection at $2\theta = 11.7^\circ$. When the Pd NCs were added into Fe-Co-Ni LDH, the relative intensity became weaker. This suggested the composite exhibited a lower crystallinity, or we could attribute to the exfoliation of LDH layers. There was no shift in the (003) reflection peak, indicating no intercalation took place in this process. As determined by the ICP-AES, the content of Pd in Pd/Fe-Co-Ni LDH was evaluated to be 3.8 wt.%, which was in good consistence with the initial incorporation of Pd (4.0 wt.%) from Na_2PdCl_4 , suggesting the efficient use of noble metals.

As shown by the field-emission SEM (FESEM) image (Fig. 2a), the shape of ZIF-67 was of typical rhombic dodecahedron [39]. A magnified image revealed smooth surfaces over the ZIF-67 crystallites



Scheme 2. The hydrogenation of 2-methyl-3-butyn-2-ol (MBY) to 2-methyl-3-buten-2-ol (MBE, semi-hydrogenation) and/or 2-methyl-2-butanol (MBA, over-hydrogenation). Other products such as isomers, dimmers were omitted due to the slight amount.

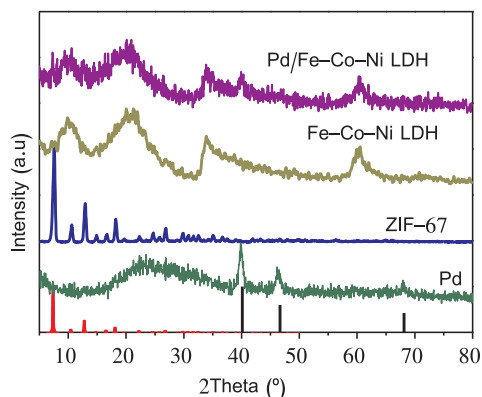


Fig. 1. XRD patterns of Pd NCs, ZIF-67, Fe-Co-Ni LDH and Pd/Fe-Co-Ni LDH.

(Fig. 2b). After solvothermal treatment with nitrates of iron and nickel, the SEM of Fe-Co-Ni LDH was given in Fig. 2c. Uniform cages were still observed, but rhombic dodecahedrons remained less regularly shaped.

This transformation might be explained by the conversion from ZIF-67 shell to Fe-Co-Ni LDH nanoflakes in hydrolysis of Fe³⁺, Ni²⁺, Co²⁺ ions (Scheme 1) during which H⁺ protons were generated to break bonds in ZIF-67. Probably part of the Co²⁺ ions in ZIF-67 were oxidized to Co³⁺ after embedding with Pd NCs [30]. The SEM image of final Pd/Fe-Co-Ni LDH was shown in Fig. 2d denoting fine textures of nanocages. Cages of Pd/Fe-Co-Ni LDH seemed to be encapsulated by flocculated substances, and layered substances were assembled with edge-to-face stacking. The prepared composite Pd/Fe-Co-Ni LDH inherited the morphology and dimension of ZIF-67 as in forms of rhombic dodecahedron.

To get more structural and compositional information, the TEM characterization linked with energy dispersive x-ray microanalysis (EDS) was carried out. Fig. 3a showed a typical TEM image of the as-synthesized ZIF-67, which exhibits as polyhedral crystallites. The single crystallites with smooth surface exhibited an average particle size of ca. 600 nm. In sample of Fe-Co-Ni LDH the flocculated nanosheets were found to assemble into cages. Facets of polyhedrons were observed to construct porous stacking. The contrast between shells and hollow interior clearly revealed the internal cavity. Insert in Fig. 3b was an enlarged TEM image given to cages as LDH nanosheets with d-spacing of

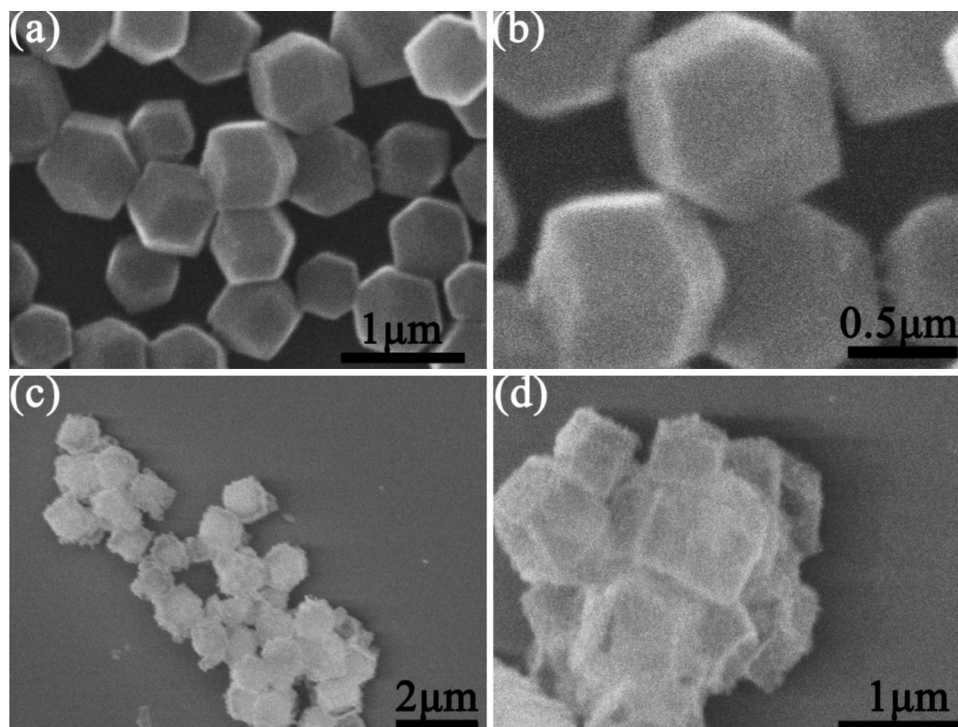


Fig. 2. SEM images of ZIF-67 (a, b), the Fe-Co-Ni LDH (c), and the final product of Pd/Fe-Co-Ni LDH with loaded Pd NCs (d).

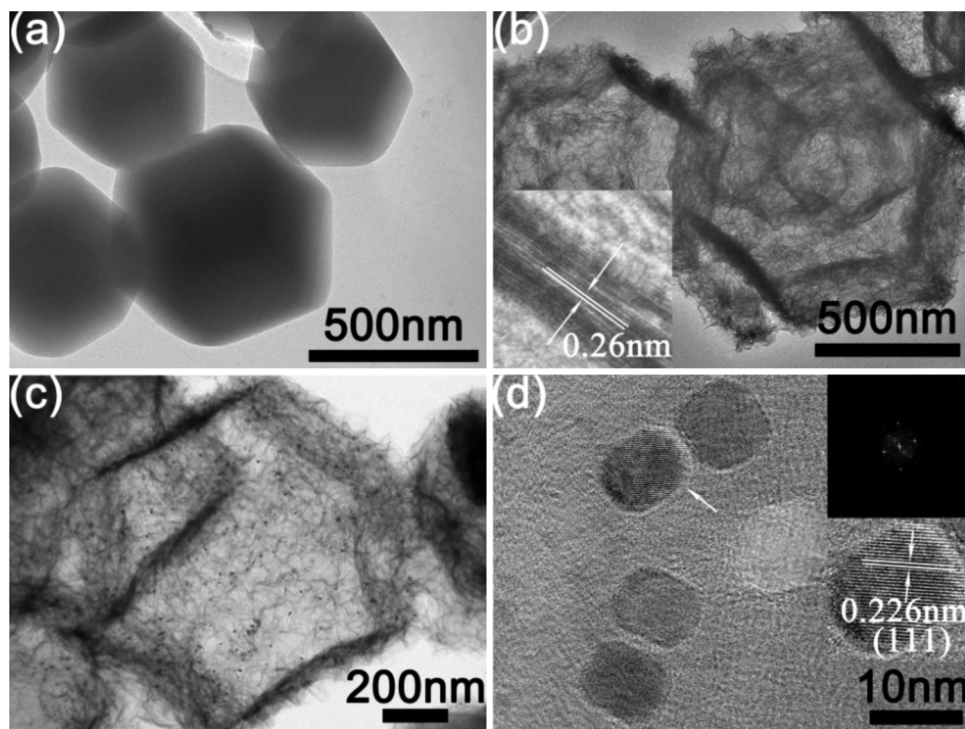


Fig. 3. TEM images of ZIF-67 (a), the as-prepared Fe-Co-Ni LDH nanocages (b), the Pd/Fe-Co-Ni LDH catalyst (c), and the HRTEM of Pd NCs (d). Insert in Fig. 3d is the fast Fourier transform (FFT) pattern.

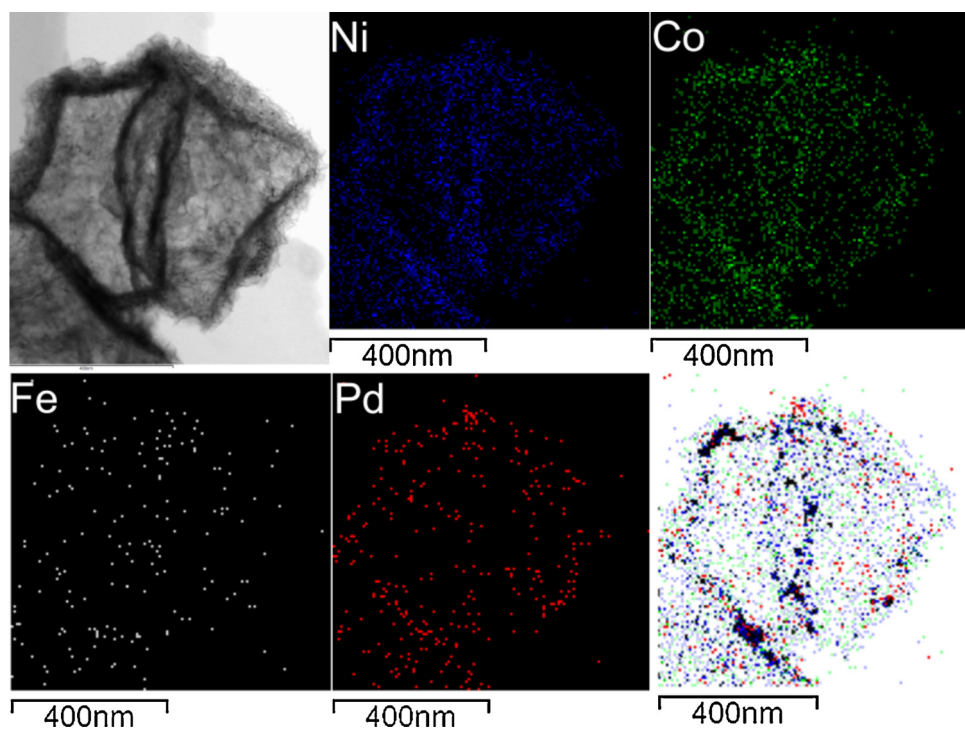


Fig. 4. STEM image and elemental mapping of an individual particle of the Pd/Fe-Co-Ni LDH hollow nanocages.

0.26 nm attributed to plane (006) of LDH. The morphology of co-precipitation LDH (Fig. S3) was layered structures with large lateral size of disorder stacking and small thickness. Fig. 3c showed the TEM image of Pd/Fe-Co-Ni LDH. Numerous particles were observed with sizes of ~10 nm, and particles were uniformly deposited on the LDH layers. The high-resolution TEM (HRTEM) image (Fig. 3d) of Pd NCs showed the interplanar spacing of 0.226 nm (inset in Fig. 3d), which agreed

with the (111) lattice spacing of face-centered cubic (fcc) Pd [40]. According to EDS analysis the content of Pd in Pd/Fe-Co-Ni LDH was evaluated to be 3.6 %, and this value was close to ICP-AES measurements. The most striking feature was the uniform sizes of Pd NCs being monodispersed on surfaces of LDH. A scanning TEM (STEM) image with EDX mapping confirmed the uniform distribution of Pd, Fe, Co and Ni throughout the hollow nanocage (Fig. 4). It was worth noting that the

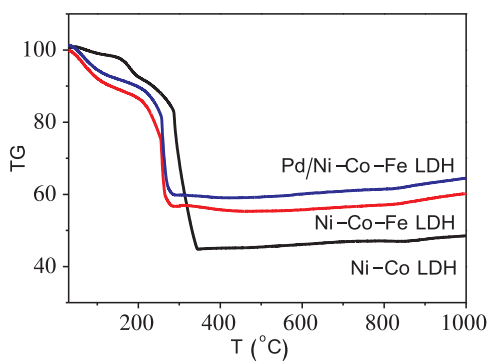


Fig. 5. Typical TG curves of Ni-Co LDH, Ni-Co-Fe LDH and final catalyst of Pd/Ni-Co-Fe LDH.

M^{3+}/M^{2+} molar ratio and solvent composition played a crucial role in the growth of Fe-Co-Ni LDH. The removal of internal templates during hydrolysis reaction was essential. The template corrosion rate could be accelerated by adding more Fe^{3+} (Fig. S4), but the growth was decreased by using ethanol as solvents. As a result, the ZIF-67 precursors were not eaten up completely, and the released Co^{2+} ions produced the Fe-Co-Ni LDH nanosheets as confirmed by EDS mapping.

The TG curves were given in Fig. 5, and all samples had three stages of weight loss. The slow trend of sample weight loss from RT to 228 °C was attributed to physically adsorbed substances, e.g., interlayer water and a small amount of free 2-methylimidazole. The next stage was removal of hydroxyl groups of the laminate and interlayer of carbonate ions. Probably the structure of laminate was collapsed to form multi-metal composite oxides. Comparing the three curves in Fig. 5, the weight loss temperature of Ni-Co LDH was terminated at 340 °C and Fe-Co-Ni LDH at 270 °C, which suggested the sample Fe-Co-Ni LDH was more difficult to remove physically adsorbed water. This might also be related to decomposition of LDH nanosheets. It was found that with increased molar ratio of M^{3+}/M^{2+} the content of removable water decreased, which could be due to the introduction of iron, exhibiting as increased d(003) reflection, and this was identified by Fig. 1. This phenomenon was also indicated to increase charge density of the LDH sheets. The more presence of M^{3+} also enhanced the hydrogen bonding of water molecules, strengthened the interaction between water molecules and interlayer carbonate ions. By comparing the weightlessness curves of Fe-Co-Ni LDH and Pd/Fe-Co-Ni LDH, the amount of Pd loaded on the nanosheets was evaluated to be 3.7 wt.%.

The FT-IR spectra of Pd NCs, ZIF-67, Ni-Co LDH, Fe-Co-Ni LDH and Pd/Fe-Co-Ni LDH were illustrated in Fig. 6. The characteristic IR bands of ZIF-67 was mainly attributed to ligand 2-methylimidazole. The band at 1580 cm^{-1} corresponded to stretching mode of the C=N bond of ligands. The stretching and bending modes of imidazole ring appeared at $600\text{--}1500\text{ cm}^{-1}$. The out-of-plane N-H...N bending and N-H

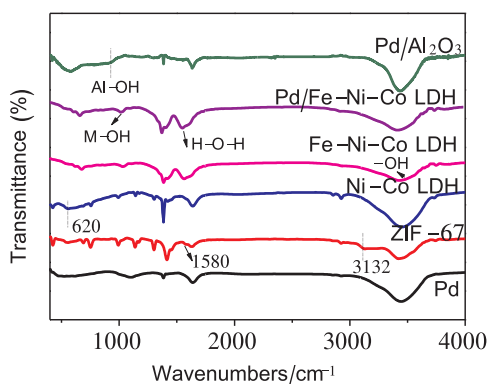


Fig. 6. FT-IR spectroscopy of the synthesized samples.

stretching in 2-methylimidazole were observed at 2670 cm^{-1} and 1849 cm^{-1} [41]. Moreover, the band at 3132 cm^{-1} was assigned to aliphatic chains. However, the band intensity of imidazole ligands decreased sharply after addition of Fe and Ni precursors. The Ni-Co LDH spectrum displayed a new broad absorption peak at about 620 cm^{-1} which was attributed to the Ni-O tensile vibration. The absorption band of Ni-O-Co had a lower wavenumber within $600\text{--}1000\text{ cm}^{-1}$. This indicated that part of the ZIF-67 templates were removed and converted to Ni-Co LDH nanosheets. The Ni-O vibration mode of NO_3^- showed an intense band at 840 cm^{-1} and 1385 cm^{-1} which decreased with formation of LDH. A broad band at 3425 cm^{-1} corresponding to stretching of hydroxyl group ($-OH$) was found to be dependent on ratios of $M^{3+}/(M^{2+} + M^{3+})$ [42]. In order to increase the content of M^{3+} , ions of Fe^{3+} were added to the synthetic LDH cages. For spectra of Fe-Co-Ni LDH, the IR bands below 900 cm^{-1} were found as the Fe-O and Fe-O-Fe vibrational modes [43]. Compared to Ni-Co LDH, modes of $\nu(M-OH)$ in Fe-Co-Ni LDH appeared at 527 , 555 and 1036 cm^{-1} [44]. The band of Fe-Co-Ni LDH at 1631 cm^{-1} was particularly observable, which was caused by the H-bound $-OH$ groups. The position of $-OH$ absorption band shifted towards lower wavenumber at 3444 cm^{-1} (vs. 3425 cm^{-1}). This was due to the trivalent cations (Fe^{3+}) that had stronger polarity bonded with $-OH$. The band around 3636 cm^{-1} was indicated to free $-OH$ groups, therefore, the addition of Fe^{3+} would enhance alkalinity of LDH. For composite Pd/Fe-Co-Ni LDH, the band of M-OH at 1036 cm^{-1} slightly shifted to 1018 cm^{-1} which can be a proof of oxidative $Pd\delta^+$ species. The interlayer hydrogen-bonded shifted to lower wavenumber at 2934 cm^{-1} , and this could be some impurity with addition of Pd NCs that resulted in disordered structure. To verify effects of hydroxyl groups on different supports as well as the catalytic performance, a comparison sample Pd/ Al_2O_3 which was prepared by loading Pd NCs on $\gamma-Al_2O_3$, was also investigated by FT-IR. As can be seen from Fig. 6 (curve Pd/ Al_2O_3), The band at 750 cm^{-1} was assigned to the stretching vibration of AlO_4 in Al_2O_3 [45], and the O-H bond was observed at $\sim 3400\text{ cm}^{-1}$. Although the position band of Al-OH in Pd/ Al_2O_3 was not shifted by comparison with Pd/Ni-Co-Fe LDH, the band of Al-OH seems to be broadened in Pd/Ni-Co-Fe. This means that the loading of Pd NCs in Pd/Ni-Co-Fe LDH could be more complicated, and the binding environment varied from that of Pd/ Al_2O_3 . It was known that metal catalysts supported on $\gamma-Al_2O_3$ delivered poor activity and selectivity unless certain promoters were added if one wanted to get better performance [46]. Suitable promoters were found as metal hydroxides, for example, the alkaline catalysts would accelerate the reaction [46]. Explanations were given as that the $-OH$ groups assisted by alkalinity provided conducive pathways for active catalyst sites, and this pathway was essential to the hydrogen activation [47]. In other literatures this was also interpreted as the adsorption/desorption balance afforded by catalyst species with aid of supports, and has been demonstrated to affect catalysis selectivity notably [48].

XPS measurements were carried out to investigate surface chemistry of the prepared samples. The wide-range XPS spectrum in Fig. 7a confirmed the presence of C, N, Fe, Co, Ni and Pd elements in sample of Pd/Fe-Co-Ni LDH. All XPS spectra were referenced to the C 1s peak at 284.8 eV. Elements of nitrogen and carbon were observed due to the presence of ligands PVP and/or ZIF templates. Fig. 7b-d displayed high-resolution XPS profiles of Fe 2p, Co 2p and Ni 2p. The measured samples were Fe-Co-Ni LDH and Pd/Fe-Co-Ni LDH as shown in each of the three figures. To illustrate the possible states of transition metals (Fe, Co, Ni, Pd) the high-resolution XPS profiles were deconvoluted using a Gaussian-Lorentzian mix function. As can be seen (dashed lines in Fig. 7b-d), the XPS bands of Fe 2p, Co 2p and Ni 2p in Pd/Fe-Co-Ni LDH were positively shifted (to higher energy) at about 1.0 eV, 0.8 eV and 1.0 eV by comparison with those in Fe-Co-Ni LDH. These shifts suggested the occurrence of strong electronic interactions when Pd NCs were introduced to the Fe-Co-Ni LDH nanocages. These unknown interactions were demonstrated to influence the binding energy of Fe, Co and Ni in LDH platelets. For example, the Fe 2p core-level spectra

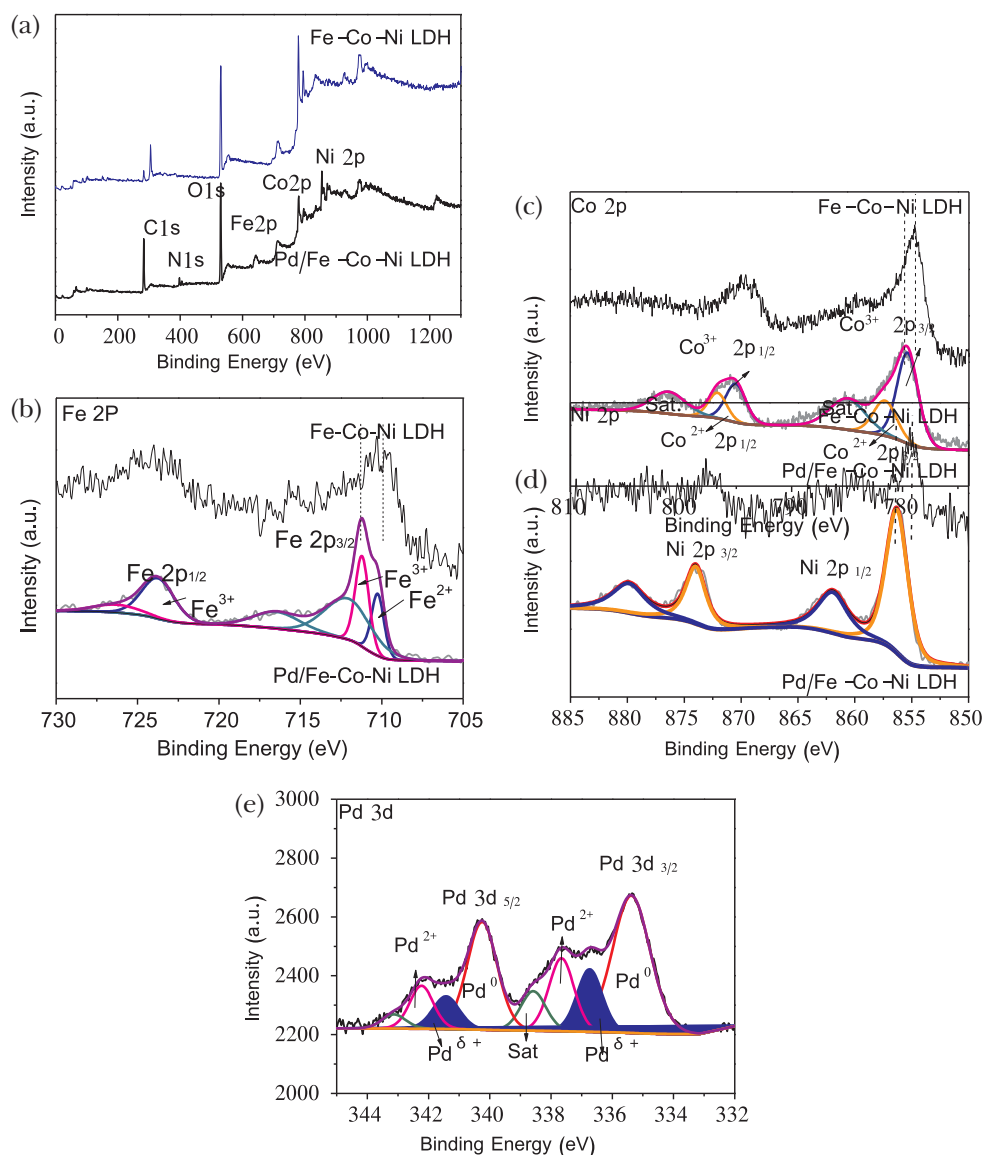


Fig. 7. (a) The wide-range survey of XPS spectra, (b) High-resolution of XPS profiles and the corresponding deconvoluted curves of Fe 2p, (c) Co 2p and (d) Ni 2p for the Fe-Co-Ni LDH and Pd/Fe-Co-Ni LDH, (e) Pd 3d in sample Pd/Fe-Co-Ni LDH.

(Fig. 7b) of Pd/Fe-Co-Ni LDH had two spin orbit peaks located at 724.3 and 710.5 eV, which could be ascribed with Fe 2p_{3/2} and Fe 2p_{1/2} of Fe³⁺. The relatively weak bands centered at 710.2 eV could be assigned to Fe²⁺. Another portion of Fe 2p band located at 723.2 eV can be attributed to the satellites [49]. The presence of iron species ensured a robust hollow nanocage and synergistic effect with the residual imidazole ligands, providing more active sites to bind with Pd NCs, which would improve catalytic performance as a result [50]. The high resolution XPS spectra of Co were displayed in Fig. 7c. As seen from the fitted curve, two sets of bands representing Co 2p_{3/2} and Co 2p_{1/2} were found at 781.5 eV ↔ 796.7 eV and 782.4 eV ↔ 797.6 eV, respectively. These two types of bands were attributed to cobalt in form of +2 and +3 oxidative states in the cobalt-doped LDH. Moreover, two extra satellite peaks appeared at 785.8 and 802.7 eV in the deconvoluted curve, which was indicative of high-spin states Co²⁺. However, this portion of Co²⁺ seems to vary due to the incorporation of Pd NCs, suggesting the Pd NCs were able to influence chemical environments of LDH as in terms of binding energy [51]. Similarly the strong peaks of Ni 2p were also observed and ascribed to Ni 2p_{3/2} and 2p_{1/2} located at 855.4 and 872.9 eV by fitting the XPS spectrum of Ni in Fig. 7d. Two shakeup satellites were observed at about 861.3 and 880.0 eV [52]. The spin-

energy separation between Ni 2p_{3/2} and Ni 2p_{1/2} being 16.2 eV could be assigned to Ni(OH)₂. The high-resolution XPS profile of Pd was shown in Fig. 7e, displaying characteristic peaks at 335.5 eV and 340.8 eV which were coincided with Pd 3d_{3/2} and Pd 3d_{5/2}, respectively. The element of Pd mainly existed in form of metallic Pd(0) with percentage of 67.45%, in minority of oxidative Pd²⁺ of 18.06%, Pd^{δ+} of 8.79% and satellites of 5.7%. There was a signal (336.0 eV) between Pd⁰ and Pd²⁺, which was found to have a shift of ~0.8 eV toward higher value vs. Pd⁰ [12,53], suggesting electron transfer from Pd NCs to LDH supports, and the Pd NCs can be immobilized by the basic sites on Fe-Co-Ni LDH. This interactions will lead to the formation of electron-deficient metal atoms (Pd^{δ+}), i.e., there is strong interactions between basic sites of supports and Pd [54]. As is known, the metal loading on a support would construct a metal-support interface, which provides an effective connection for charge transfer [55]. The reason that the state of Pd^{δ+} existed in Pd/Fe-Co-Ni LDH could be attributed to the large amount of -OH in Fe-Co-Ni LDH, and the electronegativity of -OH groups would attract more electrons from surface of Pd NCs. This interaction was confirmed by the variation of chemical environment of Fe, Co and Ni when Pd NCs were incorporated. Therefore, part of the oxidative Pd^{δ+} were indicated to appear in Pd/Fe-Co-Ni LDH [56]. These interactions

would surely enhance the dispersion of Pd and resistance to aggregation during hydrogenation, thus improving the hydrogen dissociative adsorption in semi-hydrogenation. Okhlopkova et al. [35], found that Pd NCs modified with PVP would cause XPS band shift to higher energies. Fig. S6 showed the high-resolution of XPS profiles of N 1s in sample Pd/Fe-Co-Ni LDH. Even after complete washing, the adsorbed PVP still remained on Pd NCs. In this experiment the average size of synthesized Pd NCs was ~ 10 nm. The remaining PVP after washing would provide modification of polymer molecules (PVP) on Pd NCs surface. Although partial modification by PVP deactivated the Pd catalysts, the certain extent of deactivation would favor the semi-hydrogenation, i.e., impede the over-hydrogenation. The presence of PVP prevented aggregation of Pd NCs during the reaction as well [57]. Therefore, the catalyst performance in our Pd/Fe-Co-Ni LDH was observed almost no dependence on the initial PVP/Pd ratios when the material (Pd/Fe-Co-Ni LDH) was used after washing. We indicated the change in electronic properties of Pd affected the adsorption of alkene, thereby accelerated desorption of alkene and improved the selectivity as a result [58]. The Pd element in Pd/Fe-Co-Ni LDH after reusing for 8 times was also checked (Fig. S5). The observed less amount of Pd δ^+ and increment of Pd $^{2+}$ were due to being oxidized during the cycling reactions. The XPS of the chlorine (Cl $^-$) was shown in Fig. S7. The Cl $^-$ signal was quite weak, which suggested that multiple washings after synthesis would remove Cl $^-$ ions completely.

The N $_2$ -adsorption/desorption measurements were performed to better understand structures concerning surface area and pore sizes. The Fe-Co-Ni LDH, Ni-Co LDH and ZIF-67 were used as reference samples. The template of ZIF-67 showed N $_2$ adsorption occurs under relatively low pressure, indicating that ZIF-67 was a microporous material with a Type I behavior. The specific surface area (SSA) of ZIF-67 was evaluated to be $1593.5 \text{ m}^2 \text{ g}^{-1}$ via the Brunauer-Emmett-Teller (BET) method [59]. After solvothermal treatment, the surface area of material was decreased to $83 \sim 139 \text{ m}^2 \text{ g}^{-1}$, suggesting the collapse of ZIF-67 framework and transformation into LDH platelets. The SSA of samples Fe-Co-Ni LDH and Ni-Co LDH was $139.8 \text{ m}^2 \text{ g}^{-1}$ and $83.2 \text{ m}^2 \text{ g}^{-1}$, respectively. Due to the nanocage structure, the SAA of our LDH-based material was found to be a relative high level by comparison with other's LDH materials in literatures [53]. Furthermore, the sample Pd/Fe-Co-Ni LDH with loading of Pd NCs had a SAA of $158.2 \text{ m}^2 \text{ g}^{-1}$ which was much larger than those bare LDH nanocages. This means the nano-sized Pd in LDH cages contributed to a higher surface area. In Fig. 8a the hysteresis loop of Pd/Fe-Co-Ni LDH was larger than others'. The hysteresis loop was observed for Pd/Fe-Co-Ni LDH, Fe-Co-Ni LDH and Ni-Co LDH in range of $P/P_0 = 0.4 \sim 0.8$, suggesting the hollow cages belonged to an adsorption-desorption behavior of typical IV. The uniform mesopores might come from ZIF-67 templates. The hysteresis loop at relatively high pressures ($P/P_0 > 0.9$) indicated the presence of macropores in Pd/Fe-Co-Ni LDH, which might be formed by packing of LDH sheets. The pore size distribution was

Table 1
Surface area of ZIF-67, Ni-Co LDH, Fe-Co-Ni LDH and Pd/Fe-Co-Ni LDH.

Sample	Specific surface area (m^2/g)	Average pore size (nm)
ZIF-67	1593.5	2.4
Ni-Co LDH	83.2	6.6
Fe-Co-Ni LDH	139.8	11.5
Pd/Fe-Co-Ni LDH	158.2	14.2

Table 2
Hydrogenation of MBY with different samples prepared in this work.^a

Entry	Catalyst	Time/h	Conversion	Selectivity	TOF ^b (s^{-1})
1	ZIF-67	3	3.2	–	–
2	Fe-Co-Ni LDH	3	< 1	–	–
3	Pd NCs	1	89.2	54.2	27.1
4	Pd/ZIF-67	1	78.3	49.7	23.7
5	Pd/Co-LDH	1	88.1	68.5	26.6
6	Pd/Ni-Co LDH	1	92.5	80.9	28.0
7	Pd/Fe-Co-Ni LDH	1	> 99.0	> 99.0	30.2
8	Pd/Fe-Co-Ni LDH 500 °C	1	93.6	79.6	28.3
9	Pd/Fe-Co-Ni LDH ^c	1	92.9	53.8	28.1
10	Pd/C	3	> 99.0	75.4	10.1
11	Pd/Al $_2$ O $_3$	3	85.1	38.7	8.6
12	Pd/SiO $_2$	5	80.2	40.6	4.9

^a Reaction condition: catalyst 10.0 mg with 2.0% wt. Pd, MBY 20.0 mL, initial 0.5 MPa H $_2$, T = 60 °C; Entries 9–11 were results catalyzed by commercial catalysts Pd/C, Pd/Al $_2$ O $_3$ and Pd/SiO $_2$ which purchased from Leader Catalyst, Shanghai.

^b TOF (turnover frequency) was calculated as conversion of moles of MBY per molar Pd in 1 s.

calculated by Barrett-Joyner-Halenda means in Fig. 8b. The catalyst of Pd/Fe-Co-Ni LDH showed a relatively wider distribution. The pore size distribution was found to range from 4.2 nm to 14.2 nm, and the multimodal pore-size distribution indicated pores were formed by stacking of LDH. The size of the Pd NCs is about 10 nm, while the average pore size of Fe-Co-Ni LDH support is about 11.5 nm. In this way it can be concluded that some Pd nanoparticles entered the pore channels, and this encapsulation would prevent the loss of nanoparticles during catalysis. The BET specific surface areas and pore size distribution of samples were listed in Table 1.

The catalytic performance of Pd/Fe-Co-Ni LDH for semi-hydrogenation of liquid MBY was investigated. All reactions were carried out at 60 °C, 0.5 MPa and 2000 rpm without using initiator. As a type of terminal alkynes MBY is easily over-hydrogenated to alkanes because of higher reactivity of alkynes. The catalytic performances of Pd/Fe-Co-Ni LDH and other samples (ZIF-67, Fe-Co-Ni LDH, Pd NCs, et al.) prepared was listed in Table 2. Images of gas chromatography of Pd/Fe-Co-Ni LDH reduce MBY to MBE were shown Fig. S8. The performance

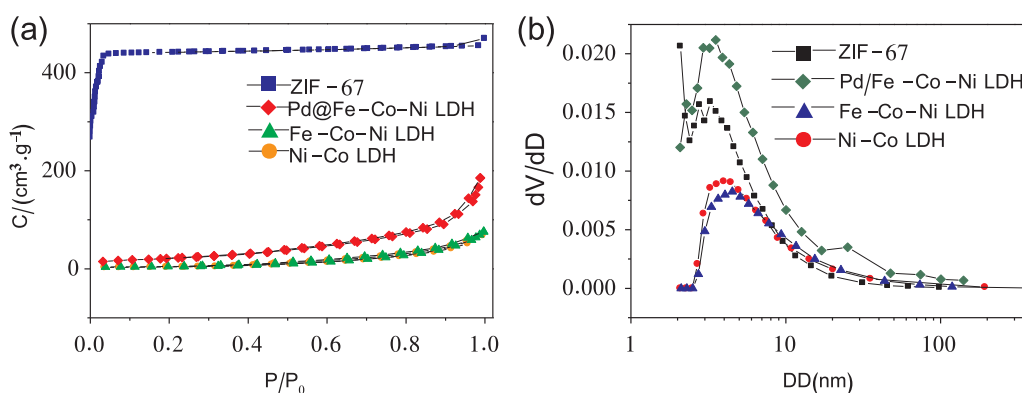


Fig. 8. (a) N $_2$ -adsorption/desorption isotherms and (b) Barrett-Joyner-Halenda of the prepared ZIF-67, Ni-Co LDH, Fe-Co-Ni LDH and Pd/Fe-Co-Ni LDH samples.

commercial Pd/C, Pd/Al₂O₃, and Pd/SiO₂ were also given in Table 2. To verify roles of supports, the Fe-Co-Ni LDH was used for hydrogenation reaction under the same condition, but no noticeable conversion of MBY was observed (Entry 2). This confirmed the Fe-Co-Ni LDH was inactive for hydrogenation catalysis without Pd NCs. For catalysis using pure ZIF-67, the amount of MBY was only observed, and almost no products were formed. The hydrogenation performance of Pd NCs to MBY was excellent, i.e., the conversion rate is 89.2%, but the selectivity is only 54.2%. This indicated that MBY on Pd catalyst was easily to be over-hydrogenated. The Pd/ZIF-67 of conversion in MBY is 78.3%, and the selectivity was 49.7%. The catalyst of Pd/Co-LDH showed a conversion of 88.1%, and the selectivity was 68.5%, suggesting the doping of Co³⁺ was beneficial to catalysis. More addition of Ni²⁺ would give synergistic effect to provide enough active sites [60], and the conversion was improved from 88.1% to 92.5%. The Pd/Fe-Co-Ni LDH had excellent performance for semi-hydrogenation of MBY to MBE by comparison with Pd/Ni-Co LDH. This suggested that Fe³⁺ had modulating effect on Ni- and Co-based LDH. To verify the effect of -OH on selective hydrogenation, the LDH supports were fully calcined at 500 °C to remove -OH from supports, catalysts were post-prepared by loading with Pd NCs. The conversion of this sample reached 93.6%, but the selectivity to MBE was only 79.6%. This demonstrates that groups of -OH in catalyst supports were important to the selectivity. The commercial Pd/C showed high activity for conversion as shown Table 2, but the selectivity was low. The selectivity of catalysts Pd/Al₂O₃ and Pd/SiO₂ were even lower, suggesting the LDH played an essential role in hydrogenation of MBY. To confirm effects of LDH on selective hydrogenation, the turnover frequency (TOF) was derived. Obviously the introduction of LDH nanocages had higher activity and selectivity in the selective hydrogenation of MBY. Although the TOF value of Pd monometallic catalyst is close to those of several types of LDH supported catalysts, the selectivity is low. Compared to other different supports, Pd/SiO₂ shows the lowest TOF which was only 0.16 times as that of Pd/Fe-Co-Ni LDH. The TOF of Pd/Al₂O₃ is 8.6 s⁻¹, and the selectivity is even lower. It is interesting that TOF of 10.1 s⁻¹ and high selectivity values were observed for Pd/C. Among the LDH support catalysts, the Pd/Fe-Co-Ni LDH has the highest TOF and selectivity. Transition metals of Fe, Co and Ni have synergistic effects with Pd NCs in hydrogenation. Moreover, the selectivity of Pd/Fe-Co-Ni LDH with hollow nano-cages for hydrogenation is much higher than LDH prepared with traditional co-precipitation under similar TOF. To evaluate the level of our prepared catalysts literatures concerning on hydrogenation of MBY were checked throughout recent publications, and the literature data were summarized in Table 3. The performance of Pd/Fe-Co-Ni was comparable to those of Lindlar catalysts (Pd-Pb/CaCO₃) [61], but our prepared Pd/Fe-Co-Ni LDH had advantages by conducting semi-hydrogenation solvent-free, and no heavy metals were used in view of avoiding potential dangers.

For the kinetics study, the Pd/Fe-Co-Ni LDH was further monitored during the hydrogenation reaction of MBY, and data of MBY conversion

and concentration of MBE, MBA were plotted versus time (Fig. 9a). The concentration of MBA tended to have an increasing trend at the early stage, and the maximum was found at about ~50 min which was followed by an almost baseline of MBA concentration (Fig. 9a). The maximum yields of MBE exceeded 99% at a conversion over 99% when the reaction time was 60 min. The over-hydrogenation of MBY to MBA was not observed before 200 min. Moreover, dimers of MBY were not observed throughout the hydrogenation. This indicated that the -OH groups of LDH in the acetylenic alcohol/enol system actually binds to Pd sites upon adsorption, thereby preventing polymerization [71]. The unique selectivity of Pd/Fe-Co-Ni LDH catalyst could be further extended to selective hydrogenation of C≡C and C=C, another experiment using a 1:1 mixture of MBY and MBE was carried out (Fig. 9b). The result showed that the only product was MBE with 99% yield, indicating that over-hydrogenation of MBE never occurred at the first stage of 200 min.

As to the recyclability, recycling runs of catalysis were carried out on Pd/Fe-Co-Ni LDH. The Pd/Fe-Co-Ni LDH displayed an extremely high stability as no deactivation was observed even after up to 8 cycling tests (Fig. 10). The conversion of MBY was found to be always higher than 99.0%, and the selectivity of MBY to MBE remained constant. To detect the loss of Pd amount in the recycling tests, samples were collected and were analyzed by the ICP-AES. The Pd loss percentage of Pd/Fe-Co-Ni LDH was < 0.5% after eight circles of reuse.

To validate the selective adsorption of MBY and MBE on catalyst supports, we used FT-IR spectrum to detect species adsorbed on the Pd/Fe-Co-Ni LDH. Pure MBY and MBE were flowed into a quartz tube at the reaction temperature (100 °C) for 60 min, and then purged with Ar flow for about 15 min to remove the gaseous and physically adsorbed MBY or MBE. As expected, bonds of C≡C and C=C were detected. Fig. 10a showed characteristic bands of MBY, MBE and MBA. The absorption peak at 2250 cm⁻¹ was a typical telescopic vibration of C≡C [72]. Other band at 1626 cm⁻¹ was assigned to the C=C [73]. It should be noted that the band of C=C was observed in Fig. 10b, which indicated the MBE group appeared on the catalyst within 30 min since the start of reaction. This might be the conversion of MBY to MBE or the adsorption of MBE on catalysts. As the reaction time was prolonged to 60 min, the competition adsorption of MBY and MBE occurred. However, the C≡C remained an stabilized state on the catalyst. Bands at 1496 and 1450 cm⁻¹ assigning to ν(C-C) of the MBA were not observed. Therefore, it could be concluded that the adsorption of C≡C on Pd/Fe-Co-Ni LDH was stronger than C=C, which favors the detachment of C=C bond in MBE instead of the C≡C in forms of MBY, resulting in hydrogenation of MBE until MBY was completely converted.

The mechanism can be drawn as that hydrogenation of alkyne firstly occurred on surface of Pd nanocubic particles, and the support acted as a co-catalyst to reduce electron density of the d-band of Pd, and thus decreased the adsorption energy of alkenes. The LDH support inhibited the formation of intermediate specie, e.g., β-palladium hydrides (β-PdH) with positively charged H-atoms, which was prone to over-

Table 3
Comparison of our prepared composite in catalysis of the MBY hydrogenation with previous reported catalysts in literatures.

Catalyst	Reaction condition	MBY Conversion	MBE Selectivity	Ref.
Pd NCs (13 nm)	333 K, 0.28 MPa, Solvent free	~97%	96%	[62]
Pd-Bi/SiO ₂	323 K, 0.1 MPa, in hexane	-	94-96%	[33]
Pd/ZnO Nanowires	333 K, 0.7 MPa,	90%	88%	[63]
PdZn/TiO ₂	313 K, 0.5 MPa, in methanol	86.5%	74.5%	[64]
PdZn/CN@ZnO	308 K, 0.5 MPa, in water	~95%	95%	[65]
Pd/Fe ₃ O ₄ /γ-Fe ₂ O ₃	363 K, 0 MPa, toluene	95.1%	97.9%	[66]
Pd ₃ S/C ₃ N ₄	303 K 0.1 MPa, toluene	~100%	100%	[67]
Pd/ZnO	343 K, 0.5 MPa	> 99%	97%	[68]
Pd-Bi/TiO ₂	335K in capillary in hexane	~95%	93 ± 1.5%	[69]
0.2 wt.%Pd/MN270	313 K, 0.3 MPa, ethanol	95%	98.7%	[70]
Pd-Pb/CaCO ₃	313 K, 0.3 MPa, ethanol	~100%	98%	[61]
Pd/Fe-Co-Ni LDH	333 K, 0.5 MPa,	~100%	99%	this work

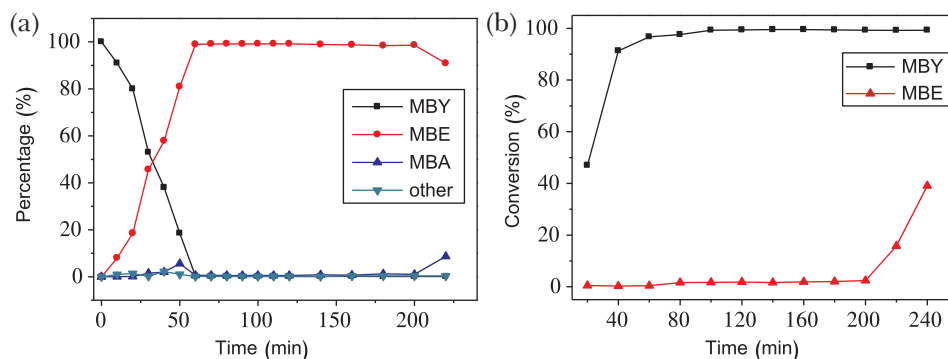


Fig. 9. (a) Percentage of MBY and products versus reaction time during hydrogenation over Pd/Fe-Co-Ni LDH catalyst. (b) The experiment using a 1:1 mixture of MBY and MBE for verifying selectivity of Pd/Fe-Co-Ni LDH catalyst.

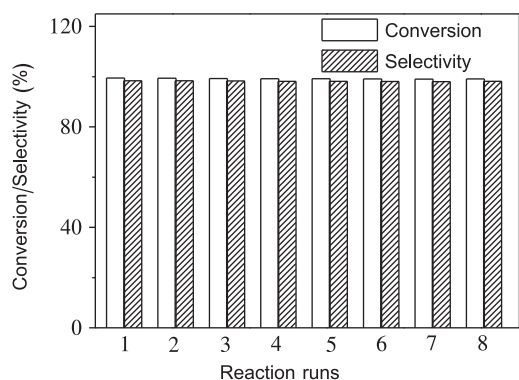


Fig. 10. Reuse of the Pd/Fe-Co-Ni LDH and reactions were conducted under conditions: $T = 60\text{ }^{\circ}\text{C}$, $P_{\text{H}_2} = 0.5\text{ MPa}$, and reaction time = 2.0 h.

hydrogenation to alkanes [74]. Due to the positively charged H-atoms the intermediate species were tended to bond with chemical groups surrounding the support. The Fe-Co-Ni LDH was assumed to have $-\text{OH}$ groups as confirmed by the IR characterization, and these groups would attract a positively charged H (Fig. 11). Therefore, the LDH inhibited the formation of $\beta\text{-PdH}$, and the semi-hydrogenation was achieved [75].

It was well known that the H_2 activation/dissociation was an important step during hydrogenation. In this research the $\text{H}_2\text{-TPD}$ experiment was carried out to investigate the H_2 -adsorption behavior on LDH based catalysts. The addition of Fe to LDH was verified to make the catalyst more prone to hydrogen dissociation and alleviate the over-hydrogenation. The $\text{H}_2\text{-TPD}$ profiles were presented in Fig. 12. As can be seen, both TPD curves of Pd/Fe-Co-Ni LDH and Pd/Co-Ni LDH were observed to have two kinds of desorption peaks. The lower temperature peak (50–150 $^{\circ}\text{C}$) represented desorption of weakly adsorbed hydrogen-

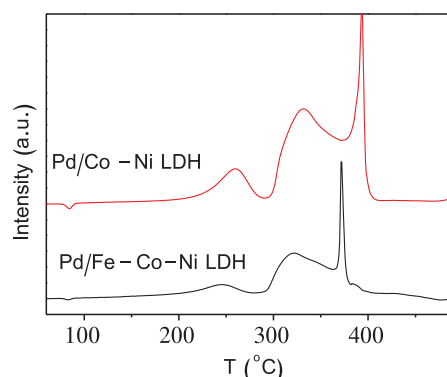


Fig. 12. $\text{H}_2\text{-TPD}$ profiles of the catalysts Pd/Fe-Co-Ni LDH and Pd/Co-Ni LDH.

species. The higher temperature peak (150–500 $^{\circ}\text{C}$) was attributed to dissociative chemisorbed hydrogen. In case of the Pd/Fe-Co-Ni-LDH, all peaks were observed at lower temperatures compared to the Pd/Co-Ni LDH. The reason lies in the introduction of Fe^{3+} which accelerate the electron transfer ability [76]. Both curves showed at least four H_2 desorption peak regions. The desorption peaks between 120–350 $^{\circ}\text{C}$ corresponded to desorption of H_2 from Pd sites onto the surface of LDH which is due to the strong interaction between Pd-LDH and H_2 at the interface sites. The peak at higher temperature was attributed to the H_2 on layers of LDH and/or spillover H_2 [77]. Compared to Pd NCs supported on Fe-Co-Ni LDH, the peak area at 394 $^{\circ}\text{C}$ for Pd/Co-Ni LDH was much larger than that of Pd/Fe-Co-Ni LDH (371 $^{\circ}\text{C}$), i.e., the weightage of this peak in all H-desorption peaks was much higher in Pd/Fe-Co-Ni LDH, thereby indicating the activation/dissociation of H_2 was more prone to occur on Pd/Fe-Co-Ni nanocages, thus contributing to improvement of activity and selectivity.

To investigate the effect of different components on catalytic

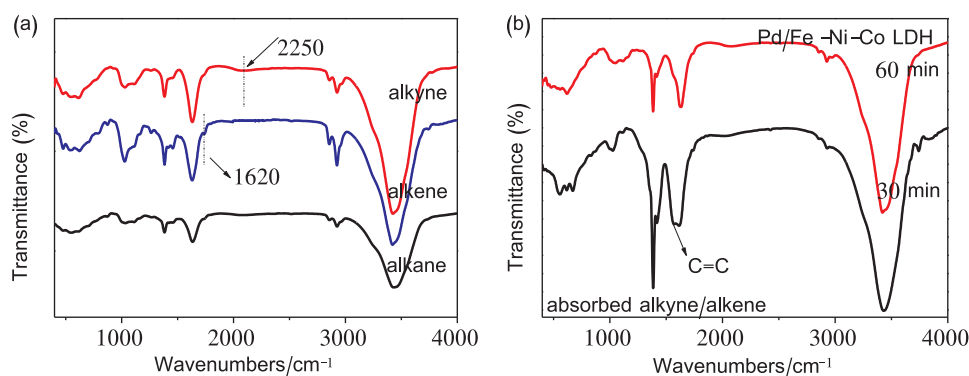


Fig. 11. (a) The FT-IR spectra of the alkyne, alkene and alkane; (b) The adsorption and desorption of alkene and alkyne for Pd/Fe-Co-Ni LDH at 30 min and 60 min.

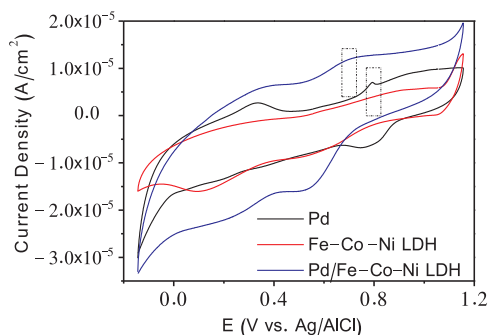


Fig. 13. CV curves of Pd, Fe-Co-Ni LDH and Pd/Fe-Co-Ni LDH in pH = 14 of KOH, 40 mV/S.

activity in Pd/Fe-Co-Ni LDH, the electrocatalytic tests of Pd, Fe-Co-Ni LDH and Pd/Fe-Co-Ni LDH were conducted in 1 M KOH by cyclic voltammogram (CV, Fig. 13). The CV of samples were carried out in potential range of $-0.14 \sim 1.14$ V vs. Ag/AgCl (saturated with KCl). The activity was evaluated by electrochemically active surface area (ECSA), i.e., the hydrogen adsorption-desorption. It was found that the ECSA of Pd/Fe-Co-Ni LDH was higher than Pd NCs or Fe-Co-Ni LDH, which suggests the Pd/Fe-Co-Ni LDH has the highest hydrogenation activity [78]. By comparison with free Pd NCs or Pd/Fe-Co-Ni LDH, the Fe-Co-Ni LDH was found to have an obvious oxidation peak within $0.8 \sim 0.7$ V and reduction potential of $0.76 \sim 0.54$ V (see the rectangular area in Fig. 13), which benefits from the reversible charge transfer to Pd in Fe-Co-Ni LDH.

4. Conclusions

In summary, a new type of catalysts based on layered double hydroxides nanocages were developed, and was successfully employed in the semi-hydrogenation of 2-methyl-3-butyn-2-ol. This catalysts have its superiority in none use of heavy metals, e.g., the doped Pb, which was always found in the previous Lindlar catalysts. The prepared Pd/Fe-Co-Ni LDH delivers brilliant performance on semi-hydrogenation of 2-methyl-3-butyn-2-ol to 2-methyl-3-buten-2-ol. Under pressure of $P_{H_2} = 0.5$ MPa at $\sim 25^\circ\text{C}$, the conversion of 2-methyl-3-butyn-2-ol reached $\sim 100\%$, and the selectivity of 2-methyl-3-buten-2-ol was higher than 99% when reactions were conducted under solventless condition. Even at prolonged reaction time, the hydrogenation product still remained at alkene. This work validates that LDH can function as supports by deliberately control of precipitation of shell materials and simultaneous etching of sacrificial templates (ZIF-67). The transition metal doped LDH, Fe-Co-Ni LDH, was demonstrated to play a vital role in suppressing the over-hydrogenation of alkynes to alkanes. The catalyst has advantage in the selective semi-hydrogenation of various alkynes by the synergy effect between Pd and Fe-Co-Ni LDH.

CRedit authorship contribution statement

Peng Zhang: Investigation, Data curation. **Ziyan Wang:** Validation. **Yan Zhang:** Software. **Jian Wang:** Visualization. **Wenqing Li:** Formal analysis. **Lina Li:** Supervision. **Peiping Zhang:** Resources. **Cundi Wei:** Project administration. **Shiding Miao:** Conceptualization, Methodology, Writing - review & editing, Funding acquisition, Supervision.

Declaration of Competing Interest

The authors declared no interests in this this work.

Acknowledgements

We acknowledged financial supports by National Natural Science Foundation of China (51874145), Open Foundation of State Key Laboratory of Mineral Processing (BGRIMM-KJSKL-2019-07), Project guide of Jilin Science and technology development plan in 2020, China Ocean Mineral Resources R&D Association (COMRA) Special Foundation (DY135-46, DY135-R2-1-01), and the Province/Jilin University co-construction project - funds for new materials - (SXGJSF2017-3).

Appendix A. Supplementary data

Supplementary material related to this article can be found, in the online version, at doi:<https://doi.org/10.1016/j.apcata.2020.117540>.

References

- [1] R. Chinchilla, C. Najera, *Chem. Rev.* 114 (2014) 1783–1826.
- [2] M. Eggersdorfer, D. Laudert, U. Letinois, T. McClymont, J. Medlock, T. Netscher, W. Bonrath, *Angew. Chem. Int. Ed.* 51 (2012) 12960–12990.
- [3] G. Vile, N. Almora-Barrios, S. Mitchell, N. Lopez, J. Perez-Ramirez, *Chem. Eur. J.* 20 (2014) 5926–5937.
- [4] M. Garcia-Mota, J. Gomez-Diaz, G. Novell-Leruth, C. Vargas-Fuentes, L. Bellarosa, B. Bridier, J. Perez-Ramirez, N. Lopez, *Theor. Chem. Acc.* 128 (2011) 663–673.
- [5] N. Semagina, M. Grasemann, N. Xanthopoulos, A. Renken, L. Kiwi-Minsker, *J. Catal.* 251 (2007) 213–222.
- [6] K.M. Engle, T.S. Mei, M. Wasa, J.Q. Yu, *Acc. Chem. Res.* 45 (2012) 788–802.
- [7] S. Zhou, L. Shang, Y. Zhao, R. Shi, G.I.N. Waterhouse, Y.C. Huang, L. Zheng, T. Zhang, *Adv. Mater.* 31 (2019).
- [8] A. Molnar, A. Sarkany, M. Varga, *J. Mol. Catal. A Chem.* 173 (2001) 185–221.
- [9] M. Tian, X. Cui, C. Dong, Z. Dong, *Appl. Surf. Sci.* 390 (2016) 100–106.
- [10] X.X. Li, Y. Pan, H. Yi, J.C. Hu, D.L. Yang, F.Z. Lv, W.D. Li, J.P. Zhou, X.J. Wu, A.W. Lei, L.N. Zhang, *ACS Catal.* 9 (2019) 4632–4641.
- [11] J. Yang, F.J. Zhang, H.Y. Lu, X. Hong, H.L. Jiang, Y. Wu, Y.D. Li, *Angew. Chem. Int. Ed.* 54 (2015) 10889–10893.
- [12] N. Iwasa, S. Masuda, N. Ogawa, N. Takezawa, *Appl. Catal. A Gen.* 125 (1995) 145–157.
- [13] S.A. Jagtap, B.M. Bhanage, *Mol. Catal.* 460 (2018) 1–6.
- [14] Y. Wan, H.Y. Wang, Q.F. Zhao, M. Klingstedt, O. Terasaki, D.Y. Zhao, *J. Am. Chem. Soc.* 131 (2009) 4541–4550.
- [15] F. Tao, M.E. Grass, Y.W. Zhang, D.R. Butcher, J.R. Renzas, Z. Liu, J.Y. Chung, B.S. Mun, M. Salmeron, G.A. Somorjai, *Science* 322 (2008) 932–934.
- [16] Z.L. Li, J.H. Liu, C.G. Xia, F.W. Li, *ACS Catal.* 3 (2013) 2440–2448.
- [17] M. Armbruster, K. Kovnir, M. Behrens, D. Teschner, Y. Grin, R. Schlogl, *Chem. Soc. Rev.* 39 (2010) 14745–14747.
- [18] W.X. Niu, Y.J. Gao, W.Q. Zhang, N. Yan, X.M. Lu, *Angew. Chem. Int. Ed.* 54 (2015) 8271–8274.
- [19] F. Studt, F. Abild-Pedersen, T. Bligaard, R.Z. Sorensen, C.H. Christensen, J.K. Norskov, *Angew. Chem. Int. Ed.* 47 (2008) 9299–9302.
- [20] P. Hauwert, G. Maestri, J.W. Sprengers, M. Catellani, C.J. Elsevier, *Angew. Chem. Int. Ed.* 47 (2008) 3223–3226.
- [21] A. Prestianni, M. Crespo-Quesada, R. Cortese, F. Ferrante, L. Kiwi-Minsker, D. Duca, *J. Phys. Chem. C* 118 (2014) 3119–3128.
- [22] J.P. Boitiaux, J. Cosyns, S. Vasudevan, *Appl. Catal.* 6 (1983) 41–51.
- [23] R. Noyori, T. Ohkuma, *Angew. Chem. Int. Ed.* 40 (2001) 40–73.
- [24] Q. Wang, D. O'Hare, *Chem. Rev.* 112 (2012) 4124–4155.
- [25] G. Fan, F. Li, D.G. Evans, X. Duan, *Chem. Soc. Rev.* 43 (2014) 7040–7066.
- [26] M. Xu, M. Wei, *Adv. Funct. Mater.* 28 (2018) 20.
- [27] Y. Tan, X.Y. Liu, L.L. Zhang, A.Q. Wang, L. Li, X.L. Pan, S. Miao, M. Haruta, H.S. Wei, H. Wang, F.J. Wang, X.D. Wang, T. Zhang, *Angew. Chem. Int. Ed.* 56 (2017) 2709–2713.
- [28] V. Holler, K. Radevik, I. Yuranov, L. Kiwi-Minsker, A. Renken, *Appl. Catal. B: Environ.* 32 (2001) 143–150.
- [29] W. Kong, J. Li, Y. Chen, Y. Ren, Y. Guo, S. Niu, Y. Yang, *Appl. Surf. Sci.* 437 (2018) 161–168.
- [30] Z. Jiang, Z. Li, Z. Qin, H. Sun, X. Jiao, D. Chen, *Nanoscale* 5 (2013) 11770–11775.
- [31] A. Berkessel, T.J.S. Schubert, T.N. Müller, *J. Am. Chem. Soc.* 124 (2002) 8693–8698.
- [32] B. Seoane, J.M. Zamoro, C. Tellez, J. Coronas, *CrystEngComm* 14 (2012) 3103–3107.
- [33] N. Cherkasov, A. Ibadon, A.J. McCue, J.A. Anderson, S.K. Johnston, *Appl. Catal. A Gen.* 497 (2015) 22–30.
- [34] M. Sudhakar, G. Naresh, G. Rambabu, C. Anjaneyulu, A.H. Padmasri, M.L. Kantam, A. Venugopal, *Catal. Commun.* 74 (2016) 91–94.
- [35] L.B. Okhlopkova, S.V. Cherepanova, I.P. Prosvirin, M.A. Kerzhentsev, Z.R. Ismagilov, *Appl. Catal. A Gen.* 549 (2018) 245–253.
- [36] Y. Sun, B. Huang, N. Xu, Y. Li, M. Luo, C. Li, Y. Qin, L. Wang, S. Guo, *Sci. Bull.* 64 (2019) 54–62.
- [37] R. Banerjee, A. Phan, B. Wang, C. Knobler, H. Furukawa, M. O'Keeffe, O.M. Yaghi,

- Science 319 (2008) 939–943.
- [38] Y. Liu, N. Wang, J.H. Pan, F. Steinbach, J.R. Caro, *J. Am. Chem. Soc.* 136 (2014) 14353–14356.
- [39] J. Tang, R.R. Salunkhe, J. Liu, N.L. Torad, M. Imura, S. Furukawa, Y. Yamauchi, *J. Am. Chem. Soc.* 137 (2015) 1572–1580.
- [40] J. Silvestre-Albero, G. Rupprechter, H.J. Freund, *Chem. Commun.* (2006) 80–81.
- [41] Y. Wang, C.Y. Wang, Y.J. Wang, H.K. Liu, Z.G. Huang, *J. Mater. Chem. A* 4 (2016) 5428–5435.
- [42] F. Cavani, F. Trifirò, A. Vaccari, *Catal. Today* 11 (1991) 173–301.
- [43] J.M. Hernandez-Moreno, M.A. Ulibarri, J.L. Rendon, C.J. Serna, *Phys. Chem. Miner.* 12 (1985) 34–38.
- [44] S. Abello, F. Medina, D. Tichit, J. Perez-Ramirez, J.C. Groen, J.E. Sueiras, P. Salagre, Y. Cesteros, *Chem.-Eur. J.* 11 (2005) 728–739.
- [45] D.M. Marinkovic, J.M. Avramovic, M.V. Stankovic, O.S. Stamenkovic, D.M. Jovanovic, V.B. Veljkovic, *Energy Convers. Manage.* 144 (2017) 399–413.
- [46] Y. Chen, X. Kong, S. Mao, Z. Wang, Y. Gong, Y. Wang, *Chin. J. Catal.* 40 (2019) 1516–1524.
- [47] S. Koukiou, M. Konsolakis, R.M. Lambert, I.V. Yentekakis, *Appl. Catal. B: Environ.* 76 (2007) 101–106.
- [48] P. Zhai, C. Xu, R. Gao, X. Liu, M. Li, W. Li, X. Fu, C. Jia, J. Xie, M. Zhao, X. Wang, W. Li, Q. Zhang, X.D. Wen, D. Ma, *Angew. Chem. Int. Ed.* 55 (2016) 9902–9907.
- [49] X. Zhu, T. Jin, C.C. Tian, C.B. Lu, X.M. Liu, M. Zeng, X.D. Zhuang, S.Z. Yang, L. He, H.L. Liu, S. Dai, *Adv. Mater.* 29 (2017) 6.
- [50] G. Jia, W. Zhang, G.Z. Fan, Z.S. Li, D.G. Fu, W.C. Hao, C.W. Yuan, Z.G. Zou, *Angew. Chem. Int. Ed.* 56 (2017) 13781–13785.
- [51] X.W. Teng, D. Black, N.J. Watkins, Y.L. Gao, H. Yang, *Nano Lett.* 3 (2003) 261–264.
- [52] Q. Wang, X. Wang, C. Shi, *Ind. Eng. Chem. Res.* 57 (2018) 12478–12484.
- [53] S. Zhao, K. Li, S. Jiang, J. Li, *Appl. Catal. B: Environ.* 181 (2016) 236–248.
- [54] Z. Xu, D.V. Cuong, Y. Liu, W. Baaziz, B. Li, N.D. Lam, O. Ersen, P.H. Cuong, *Appl. Catal. B: Environ.* 244 (2019) 128–139.
- [55] F. Su, L. Lv, F.Y. Lee, T. Liu, A.I. Cooper, X.S. Zhao, *J. Am. Chem. Soc.* 129 (2007) 14213–14223.
- [56] R.G. Rao, R. Blume, T.W. Hansen, E. Fuentes, K. Dreyer, S. Moldovan, O. Ersen, D.D. Hibbitts, Y.J. Chabal, R. Schloegl, J.P. Tessonnier, *Nat. Commun.* 8 (2017) 340.
- [57] A. Yarulin, I. Yuranov, F. Cardenas-Lizana, P. Abdulkina, L. Kiwi-Minsker, *J. Phys. Chem. C* 117 (2013) 13424–13434.
- [58] H. Hirai, N. Yakura, *Polym. Adv. Technol.* 12 (2001) 724–733.
- [59] W.L. Ji, Z.L. Xu, P.F. Liu, S.Y. Zhang, W.Q. Zhou, H.F. Li, T. Zhang, L.J. Li, X.H. Lu, J.S. Wu, W.N. Zhang, F.W. Huo, *ACS Appl. Mater. Interfaces* 9 (2017) 15394–15398.
- [60] H. Pourfarzad, M. Shabani-Nooshabadi, M.R. Ganjali, H. Kashani, *Electrochim. Acta* 317 (2019) 83–92.
- [61] B. Tripathi, L. Paniwnyk, N. Cherkasov, A.O. Ibadon, T. Lana-Villarreal, R. Gomez, *Ultrason. Sonochem.* 26 (2015) 445–451.
- [62] N. Semagina, A. Renken, D. Laub, L. Kiwi-Minsker, *J. Catal.* 246 (2007) 308–314.
- [63] L.N. Protasova, E.V. Rebrov, K.L. Choy, S.Y. Pung, V. Engels, M. Cabaj, A.E.H. Wheatley, J.C. Schouten, *Catal. Sci. Technol.* 1 (2011) 768–777.
- [64] L.B. Okhlopko, S.V. Cherepanova, I.P. Prosvirin, M.A. Kerzhentsev, Z.R. Ismagilov, *Appl. Catal. A Gen.* 549 (2018) 245–253.
- [65] L.F. Shen, S.J. Mao, J.Q. Li, M.M. Li, P. Chen, H.R. Li, Z.R. Chen, Y. Wang, *J. Catal.* 350 (2017) 13–20.
- [66] R. Easterday, C. Leonard, O. Sanchez-Felix, Y. Losovyj, M. Pink, B.D. Stein, D.G. Morgan, N.A. Lyubimova, L.Z. Nikoshvili, E.M. Sulman, W.E. Mahmoud, A.A. Al-Ghamdi, L.M. Bronstein, *ACS Appl. Mater. Interfaces* 6 (2014) 21652–21660.
- [67] D. Albani, M. Shahrokhi, Z.P. Chen, S. Mitchell, R. Hauert, N. Lopez, J. Perez-Ramirez, *Nat. Commun.* 9 (2018) 11.
- [68] M. Crespo-Quesada, M. Grasmann, N. Semagina, A. Renken, L. Kiwi-Minsker, *Catal. Today* 147 (2009) 247–254.
- [69] N. Cherkasov, A.O. Ibadon, E.V. Rebrov, *Lab Chip* 15 (2015) 1952–1960.
- [70] L. Nikoshvili, E. Shimanskaya, A. Bykov, I. Yuranov, L. Kiwi-Minsker, E. Sulman, *Catal. Today* 241 (2015) 179–188.
- [71] S. Mao, B. Zhao, Z. Wang, Y. Gong, G. Lü, X. Ma, L. Yu, Y. Wang, *Green Chem.* 21 (2019) 4143–4151.
- [72] A.A. Titov, V.A. Larionov, A.F. Smol'yakov, M.I. Godovikova, E.M. Titova, V.I. Maleev, E.S. Shubina, *Chem. Commun.* 55 (2019) 290–293.
- [73] S. Saikia, P. Gogoi, A.K. Dutta, P. Sarma, R. Borah, *J. Mol. Catal. A: Chem.* 416 (2016) 63–72.
- [74] D. Deng, Y. Yang, Y. Gong, Y. Li, X. Xu, Y. Wang, *Green Chem.* 15 (2013) 2525–2531.
- [75] K. Radkowski, B. Sundararaju, A. Fuerstner, *Angew. Chem. Int. Ed.* 52 (2013) 355–360.
- [76] Y.K. Jin, G.H. Sun, F. Xiong, L.B. Ding, W.X. Huang, *Chem.-Eur. J.* 21 (2015) 4252–4256.
- [77] Y. Cesteros, P. Salagre, F. Medina, J.E. Sueiras, *Appl. Catal. B: Environ.* 25 (2000) 213–227.
- [78] E. Rafiee, M. Kahrizi, F. Farjami, P. Dorraji, *Electrochim. Acta* 253 (2017) 1–10.